First evidence for large earthquakes on the Deshir Fault, Central Iran Plateau

H. Nazari, M. Fattahi, Bertrand Meyer, Michel Sébrier, M. Talebian, M. Foroutan, Kristell Le Dortz, M.D. Bateman, M. Ghorashi

First evidence for large earthquakes on the Deshir Fault, Central Iran Plateau

Nazari H. [1], Fattahi M. [2,3,4], Meyer B. [5], Sébrier M. [5], Talebian M. [1], Foroutan M. [1], Le Dortz K. [5], Bateman M. D. [3], and M. Ghorashi [1].

1: Institute for Earth Sciences, Geological Survey of Iran, Po Box:13185-1494,Teheran-Iran.
email: nazari@gsi-iran.org, talebian@gsi-iran.org, foroutan@gsi.ir, ghorashi@gsi-iran.org
2: The Institute of Geophysics, University of Teheran, Teheran, Iran.
email: mfattahi@ut.ac.ir
3: Sheffield Centre for International Drylands Research, Department of Geography, University of Sheffield, Winter Street, Sheffield S10 2TN, UK
email: M.D.Bateman@Sheffield.ac.uk
4: Oxford University Center of Environment South Parks Road,Oxford, OX1 3QY,England
email : morteza.fattahi@ouce.ox.ac.uk
5 : UPMC Univ Paris 06, ISTEP (UMR 7193 CNRS), F75005, Paris, France
email: bertrand.meyer@upmc.fr, michel.sebrier@upmc.fr, kristell.le_dortz@upmc.fr

short title: Large earthquakes on the Deshir Fault, Central Iran

Abstract

Although sliced by several strike slip faults, a large part of Central Iran remained aseismic during the period of time covered by the instrumental and historical seismic records. Stating the existence of earthquakes in the Holocene is therefore important for the assessment of the regional seismic hazard. A paleoseismic study of the Deshir fault demonstrates that Central Iran hosted large earthquakes during latest Pleistocene and Holocene. The last event corresponds to 1m-deep fissures which sandy infilling yielded an optically stimulated luminescence (OSL) age of 2.8±1.4 ka. At least two previous events, outlined by older fissures and/or colluvial wedges, have been recorded over the last 10-30 ka. The magnitudes are difficult to assess because the actual slips per event are unknown. The size of the fissures and the significant vertical displacement associated to a colluvial wedge are nevertheless compatible with M≈7 events along a primary strike-slip surface break.

Introduction and geological setting

The Deshir Fault is the westernmost prominent N-striking dextral strike-slip fault of a series that slice Central and Eastern Iran (e.g.; Berberian, 1981; Walker and Jackson, 2004; Meyer and Ledortz, 2007; inset, Figure 1). The fault locates North of the Zagros, nearby 54°E, and cuts across an area of the Central Iran Plateau devoid of instrumental and historical seismicity (Ambraseys and Melville, 1982; Ambraseys and Jackson, 1998). Despite the lack of seismicity in its vicinity and the absence of resolvable deformation by the GPS network in Central Iran over two (Vernant et al., 2004) and six (Masson et al., 2007) years, the fault has long been suggested active (e.g., Berberian, 1981). There is now morphologic evidence for it and right-lateral offsets document a cumulative fault-slip of ~25m at several sites along the fault (Meyer et al., 2006). However, the Holocene time-period over which it surmised to have accumulated remains questionable. Although Meyer et al. (2006) suggested small stream offsets of 4-5m to the south of Marvast might result from coseismic slip during an earthquake of unknown age and magnitude ~7, the seismic behaviour of the Deshir fault is still not assessed. Trenching appears therefore appropriate to document Holocene earthquakes, if there were any, in a region that long remained quiescent according to the seismic records.

The information on the geometry and overall fault morphology is summarized from Meyer et al. (2006). The Deshir fault is a 380-km long straight strike-slip fault involving several portions (Figure 1). The northern portion, located between Nain and Deshir, disrupts the western part of the Nain-Baft suture and cuts across the Urumieh Doktar magmatic arc.

The southern 230-km-long portion extends between Deshir and Harat, and cuts the eastern part of the Nain-Baft suture. The piercing points of the suture are difficult to pinpoint and estimates of the total dextral offset range between 50 and 80 km. South of Deshir, the fault trends N150-160 and runs obliquely across coalescent fans that merge with Quaternary salt flat depressions. Within the salt flats, the fault intersects marshes along an ill-defined scarp. Through the coalescent fans, the fault bears a clear 2- to-20 m high cumulative scarp depending on the relative ages of the fans, and its prevalent dextral motion is attested by deflected river courses and offsets of terrace-risers. We scrutinized the southern fault portion on SPOT imagery and in the field, searching for the favourable places to conduct paleoseismic investigations and document the seismic history of the fault. We excavated trenches at three sites several tens of kilometres apart. Two revealed evidences of paleoseismic events. The third revealed unsuitable and showed distributed shear across steeply-dipping neogene units without convincing evidences of deformation of the thin discontinuous aeolian sands mantling the Neogene. We report here the observations gathered at the northernmost site where the lithology allowed us to unambiguously distinguish several events.

The trench site and the excavation

The excavation site is located North of Marvast where the fault cuts across a large intermittent stream that supplies water to the Deshir salt flat. Except for the main river flood plain where it has been eroded, the fault scarp is readily seen on the SPOT imagery and well expressed in the field (Figure 2). The scarp is less than 2m-high, faces to the east, and delineates a subtle depression or furrow associated to prevalent strike-slip motion. Tiny morphological features are well resolved on the right bank of the river where the fault cuts across an abandoned fan surface. Several ephemeral gullies denoted by grey linear areas have incised the fan surface to join the active flood plain. The gullies have probably formed as a result of regressive erosion since the last significant incision of the network. Close to the main river flood plain, one such gully, less than 200m long, flows nearby and parallel to the fault. Further to the south, the fault intersects at right angle several gullies, a few tens to a few hundreds of meters long. The right-lateral offset of the two gullies to the south amounts to 25±5m. In between the smallest of the gullies intersecting the fault and the upper reaches of the gully paralleling it, there is a 30-50m long section of the scarp preserved from recent erosion (Figures 2,3a). The smooth scarp delineates a subdued, 10-20m wide, 1.5m deep,

depression denoted by white patches on the SPOT image (Figure 3b). These white patches outline the accumulation of a thin layer of silts and clays washed out from the scarp during episodic surface runoff. We discuss the most elucidating wall of a 25m long, 2m wide, 4m deep trench excavated across this depression.

Trench stratigraphy

The trench wall (Figure 4) exhibits highly disrupted, coarse Quaternary deposits so that unit correlations across fault splays (f1 to f6) may be questionable. The overall structure of the trench corresponds to an asymmetric sag, limited to the east by the main fault zone (MFZ) and to the west by the f1 fault. The latter has controlled the development of the east-facing scarp that delineates the Deshir fault along several tens kilometres on the satellite imagery (Figures 1, 2). The eastern part of the trench is a tilted block, which extends between the MFZ and the easternmost faults (f5, f6). The overall structure thus suggests that the most recent deposits should have been trapped in the central part of the sag between f1 and f2. Despite the difficulties correlating units across individual faults, the overall stratigraphy is made of two main bodies of units: (1) older alluvial fanglomerates (blue colours, Figure 4) and (2) younger alluviums and colluviums (non-blue colours). The units have been described separately within the different blocks (Table 1 and Figure 4) and named accordingly with different letters (A to E) followed by a numbering order from bottom to top. Older units (A1, C1, D1, and E1) are exposed on both edges and in the lower part of the trench. They correspond to distal alluvial fan deposits that were probably shed by the Marvast River during Quaternary. Younger units of more local origin are exposed in the centre and the upper part of the trench and constst of:

(1) alluviums (A2, D2, D3, D4) corresponding to surface runoff sediments emplaced by short streams and small channels reworking older units and flowing mainly parallel to the fault. Such a network has probably been similar to the current second-order streams (Figure 2a).

(2) muddy deposits corresponding to distal surface runoff material (B1, B2).

(3) colluviums corresponding to desert cover (A3, C2, 7), colluvial wedge (D5), or fissure fills (D6, part of unit 7).

The stratigraphy has been constrained in age using Optically Stimulated Luminescence (OSL, Table 2). Although most ages have large uncertainties precluding accurate unit correlations, the ages indicate that unit 7 is Late Holocene (Marine Isotopic Stage MIS-1)

while B2 and B1 are approximately coeval with MIS-2 (≈12-22 ka) and MIS-3 (≈22-59 ka), respectively. Then, D5, D6, and possibly C2 and A3 correlate with B2 (MIS2) whilst D4, D3, Dx, and possibly A2 correlate with B1 (MIS-3). Aggradation of older alluvial units A1, C1, D1 and E1 occurred partly during MIS-4 (≈59-80 ka). Finally, the calcrete formation should be of Early-Middle Holocene age, as the youngest deposits (unit 7, 2.8±1.4ka) do not contain calcretes.

Seismic event identification

The excavation evidences that coseismic surface ruptures have occurred repeatedly on the Deshir fault. The youngest event (ev1; Figures 4,5,6a) corresponds to open cracks and fissures filled by unit 7 and to the sealing unconformity on the Main Fault Zone. Indeed, a western MFZ splay, sealed by unit 7 whose thickness rapidly decreases eastward, indicates the occurrence of a small step prior to unit 7, hence a surface break coeval with ev1. The largest fissures are recognized on the two walls of the trench; they strike N170-180 obliquely to the N160 fault zone and to the slope of the scarp, as expected for dextral en echelon tension gashes. These fissures are remnants of en echelon cracks along a primary dextral tectonic break. They postdate A3 and subsequent calcrete cementation and predate 7 not cemented by the calcrete. OSL dating within the infill of one of these fissures indicates that the causative seismic event occurred prior to 2.8±1.4 ka. Since the sandy-silty material that fills the fissure has a significant aeolian component, it was probably emplaced shortly after the earthquake during winter dust storm and the OSL age of the infill provides a likely estimate of the time of the earthquake. The event horizon, predating unit 7, is distinguished all along the trench. In contrast, older events are difficult to correlate across the entire trench. They are described in each block and identified with the letters T to Z on Figure 4.

In the central sag and West block, west of f2, two additional event horizons may be identified below the ev1 horizon: evZ predates B2 and postdates B1 since the base of B2 is filling a fissure along the upper termination of f1 (Figure 6b); evY predates A2 and postdates A1 as the base of A2 appears to be filling fissures within A1. Three OSL ages indicate that evZ should have occurred between 20.5 and 28.2 ka and evY prior to 28.2 ka. Older seismic events may have occurred during B2 aggradation as this unit appears sealing f2 fault splays. However, their corresponding event horizons are not clearly identified within B2 unit.

Four additional event horizons may be identified below ev1, between f4 and f5 in the Eastern tilted zone: evV, evU, evW, and evT. EvV predates D6 fissure fill and postdates D5. Since

171 D6 is cemented by the same calcrete to D5, evV cannot correspond to ev1, and therefore must
172 postdate the calcrete. If EvU predates the D5 colluvial wedge (Figure 6d) and postdates D4,
173 then evV and evU should correspond to surface breaks reactivating f5 between 2.8±1.4 ka and
174 21.1±11.2 ka.
175 The two older events, evW and evT, are ill-defined. EvW may correspond to a small
176 crack splaying off fault f5 and sealed by D4 unit. If this is the case then it have occurred
177 between 21.1±11.2 ka and 34.6±17.5 ka. EvT is extrapolated from the Western tilted zone
178 where the D2-D3 limit is an event horizon.
179 Three event horizons may be identified below ev1 in the Western tilted zone between
180 f3 and f4: evX predates C2 and postdates Dx. Indeed, the boundary between Dx and C2
181 appears as an event horizon as C2 is sealing f3 and most of the MFZ. Event evW would
182 predate Dx and postdate D3, as the base of Dx appears filling a fissure along f4. EvT,
183 predating D3 and postdating D2, corresponds to the sealing unconformity of a f3 fault splay
184 with drag fold by D3 (Figure 6c). The OSL age of Dx indicates that evX postdates while evW
185 and evT predate 41.5±15.9 ka. Only two events, ev1 and evX, can be identified in the MFZ.
186 Considering available ages, there is no simple correlations for events prior to ev1. Two
187 options may be contemplated for the penultimate event that occurred between 20.5 and 28.2
188 ka: (1) evV could correlate with evX and evZ, also seen as the penultimate event in their
189 respective blocks or (2) evV is not present to the west of f4 fault and then, evU, evX, and evZ
190 may correspond to the same event. Correlations for older events are only speculative: evW is
191 ill-defined, inaccurately dated between 9.8 and 52.1 ka, and not recognized to the west of the
192 MFZ; evT, which predates 34.6±17.5 ka and 41.5±15.9 ka, might correlate with evY.
193
194 **Conclusions**
195 Paleoseismic data give evidence for a maximum of five earthquakes on the Deshir
196 fault during latest Pleistocene-Holocene. OSL dating constrains the late last three events to
197 the last 21.1±11.2 ka, suggesting a rough return period of 7±4 ka. The time elapsed since the
198 last earthquake likely ranges between 1.4 to 4.2 ka *[1]. The corresponding magnitudes,
199 specifically for strike-slip earthquakes in a single trench, remain difficult to assess because the
200 actual slip per event is not accessible. It is nonetheless possible to place loose constraints on
201 the size of two earthquakes. For the antepenultimate event, evU, the thickness of the colluvial

201

[1] During the review process of this manuscript, a subsequent study of a small subset of the OSL data explored non-standard methods and unconventional statistical tests to narrow the error bars and has resulted in a refined likely age of 2.0 ± 0.2 ka for the last earthquake (Fattahi et al., 2009).

wedge D5 indicates significant (≈1m) vertical offset, hence large (several metres) horizontal displacement, along a primary strike-slip break and appears compatible with an event of magnitude M>6.5. For the last event, the deep fissures in the trench are much larger than the small fissures observed along the tiny surface break of the 2003 M=6.5 Bam earthquake (Jackson et al., 2006). They rather compare with the prominent open fissures mapped along the 150km-long portion of the North Anatolian Fault broken by the Mw=7.6 Izmit (Barka et al., 2002) and Mw=7.2 Dücze (Akyuz et al., 2002) earthquakes. Accordingly, the last event evidenced in the trench might have been of magnitude M≥7 and large enough to account for the small stream offsets of 4-5 m documented by Meyer et al. (2006) only 30 kilometres to the South of the trench. Moreover, the gullies incised within the fan surface postdate the whole set of alluvial and colluvial units and yield a minimum slip-rate on the order of 0.8-2.5 mm/yr, assuming their 25m offset is at most 21.1±11.2 ka (age of D4, youngest colluviums predating the abandonment of the fan surface and subsequently incised by streams flowing through the fault zone).

Although providing rough estimates on the recurrence and loose constraints on the magnitude of earthquakes, such studies are the only conceivable way for assessing seismic hazard in regions where the seismic cycle spans a period of time longer than that accessible to instrumental and historical seismic records, as is the case of Central Iran. Several other faults, that are now recognized as active (e.g., Meyer et al., 2007; Walker, 2008) but whose seismic behaviour remains unknown, require a better description of the current tectonics and an appropriate hazard assessment by trenching and application of chronological control.

Acknowledgments.

This study benefited from logistic and financial assistance from Geological Survey of Iran. UPMC-Paris6, INSU-CNRS, and CNES-SPOT Image (ISIS0403-622, ISIS0510-812) provided complementary funding. KL received a Ministry of Research and Education scholarship granted by the President of UPMC. We acknowledge constructive criticisms by F. Cinti, J-F. Ritz, R. Walker, and one anonymous reviewer. Editor and Associate Editor, C. Doglioni and H. Pedersen, provided helpful suggestions.

References

Akyüz, H.S., R. Hartleb, A. Barka, E. Altunel, G. Sunal, B. Meyer, R. Armijo and J.B. de Chabalier, (2002). Field observations and slip distribution of the November 12, 1999 Düzce earthquake (M=7.1), Bolu-Turkey, *Bull. Seism. Soc. Am.*, special volume 92, 61-66.

236 Ambraseys, N. and Melville, C. (1982). A history of Persian earthquakes. Cambridge University Press.
237 Ambraseys, N.N. & Jackson, J.A (1998). Faulting associated with historical and recent earthquakes in
238 the Eastern Mediterranean region. *Geophysical Journal International* , 133, 390-406.
239 Barka, A., H.S . Akyüz, G. Sunal, Z. Cakir, A. Dikba, B. Yerli, R. Armijo, B. Meyer, J.B. de
240 Chabalier, T. Rockwell, J.R. Dolan, R. Hartleb, T. Dawson, S. Christofferson, A. Tucker, T.
241 Fumal, R. langridge, H. Stenner, W. Lettis, J. Bachhuber and W. Page (2002). The August 17,
242 199 Izmit earthquake, M=7.4, Eastern Marmara region, Turkey : study of surface rupture and slip
243 distribution, *Bull. Seism. Soc. Am*., special volume 92, 43-60.
244 Bateman, M.D. and Catt, J.A. (1996). An absolute chronology for the raised beach and associated
245 deposits at Sewerby, East Yorkshire, England. *Journal of Quaternary Science*, 11(5), 389-395.
246 Berberian, M. (1981). Active faulting and tectonics of Iran. In: Gupta, H. and Delany, F. (editors),
247 Zagros-Hindu Kush-Himalaya Geodynamic Evolution, Geodynamic Series, Chapter 3, 33–69.
248 American Geophysical Union.
249 Fattahi, M., Walker, R., Hollingsworth, J., Bahroudi, A., Talebian, M., Armitage, S. and Stokes, S.
250 (2006) Holocene slip-rate on the Sabzevar thrust fault, NE Iran, determined using Optically-
251 stimulated Luminescence (OSL). *Earth and Planetary Science Letters*, 245: 673-684.
252 Fattahi, M., Walker, R., Khatib, M.M., Dolati, A. and Bahroudi, J. (2007) Slip-rate estimates and past
253 earthquakes on the Doruneh fault, eastern Iran. *Geophysical Journal International*, 168: 691-709.
254 Fattahi, M., Nazari, H., Bateman, M.D., Meyer, B., Sébrier, M., Talebian, M., Le Dortz, K., Foroutan,
255 M., Ahmadi Givi, F., and M. Ghorashi (2009). Refining the OSL age of the last earthquake on the
256 Dheshir fault, Central Iran, in press, *Quaternary Geochronology*.
257 Jackson J., Bouchon M., Fielding E., Funning G., Ghorashi M., Hatzfeld D., Nazari H., Parsons B.,
258 Priestley K., Talebian M., Tatar M., Walker R., and Wright T. (2006) Seismotectonic, rupture
259 process, and earthquake-hazard aspects of the 2003 December 26 Bam, Iran, earthquake.
260 *Geophysical Journal International* 166(3), 1270-1292
261 Masson, F., M. Anvari, Y. Djamour, A. Walpersdorf, F. Tavakoli, M. Daignières, H. Nankali, S. Van
262 Gorp (2007) Large-scale velocity field and strain tensor in Iran inferred from GPS measurements:
263 new insight for the present-day deformation pattern within NE Iran, *Geophysical Journal*
264 *International*, 170 (1), 436–440. doi:10.1111/j.1365-246X.2007.03477.x
265 Meyer, B., F. Mouthereau, O. Lacombe and P. Agard (2006), Evidence of Quaternary activity along
266 the Deshir fault: implication for the Tertiary tectonics of Central Iran, *Geophysical Journal*
267 *International*., 164, 192-201.
268 Meyer, B., and K. Le Dortz (2007), Strike-slip kinematics in Central and Eastern Iran: Estimating fault
269 slip-rates averaged over the Holocene, *Tectonics*, 26, TC5009, doi:10.1029/2006TC002073.
270 Murray, A.S. and Wintle, A.G., 2000. Luminescence dating of quartz using an improved single-aliquot
271 regenerative-dose protocol. *Radiation Measurements*, 32(1): 57-73.

Vernant, Ph., F. Nilforoushan, D. Hatzfeld, M.R. Abassi, C. Vigny, F. Masson, H. Nankali, J. Martinod, A. Ashtiani, R. Bayer, F. Tavakoli, and J. Chery (2004), Present-day crustal deformation and plate kinematics in the Middle East constrained by GPS measurements in Iran and Northern Oman, *Geophys. J. Int.*, 157, 381-398.

Walker, R. and J. Jackson (2004), Active tectonics and late Cenozoic strain distribution in Central and Eastern Iran, *Tectonics*, 23, TC5010, doi:10.1029/2003TC001529.

Walker, R. (2008), A remote sensing study of active folding and faulting in southern Kerman province, S.E. Iran. *Journal of Structural Geology, 28, 654-668.*

Figure captions

Figure 1: Simplified sismotectonic map of the Deshir fault. 1973-2008 seismicity from NEIC (http://neic.usgs.gov/neis/epic/). Background image is from SRTM data (http/:edcsgs9.cr.usgs.gov/pub/data/srtm/) supplemented with Landsat images for unfilled areas (mostly lakes and salt flats). Red square for location of figure 2. Insert locates the area within the simplified seismotectonic map of Iran. Red arrows are GPS velocities with respect to stable Eurasia (Vernant et al., 2004; Masson et al., 2007).

Figure 2: The excavation site. (a) SPOT satellite extract highlighting fault trace on both sides of a main river flood plain which tributaries have incised an abandoned fan. Right-lateral offset of two small gullies (circled area) is 20-30 m. Rectangle 3a and line 3b respectively locate 3-D enlargement and section in figure 3. T indicates position and approximate extent of analyzed trench. Right panels show enlargements of raw (top) and interpreted (bottom) images of the offset gullies. (b) Field photograph of the N160 linear, east-facing, 2m-high scarp. View is taken to the south from the eastern tip of the trench. Cars parked by the base of the scarp for scale.

Figure 3: a, 3-D perspective view of the excavation site obtained from draping a HR Quickbird image on a Digital Elevation Model worked out from a differential GPS survey. b, Topographic profile (VE~14) across the fault zone with dots indicating the density of the GPS survey. A depression outlines the strike-slip fault and a gentle warping to the East possibly reflects blind thrusting and upper slip partitioning of a slightly transpressive motion at depth. Box is projection of the excavated area in Figure 4.

306 **Figure 4**: Photo-mosaic of the southern wall of the trench (top), corresponding log with
307 position of dated samples (middle), and simplified stratigraphy with emplacement of seismic
308 event horizons (bottom). Boxes on upper panels locate the detailed photographs of figure 6.
309 Colour variation and mismatch in the mosaic result from assembling more than 350
310 photographs. Sedimentary units are indicated by different colours and labelled numerically
311 from bottom to top. See Table 1 for detailed description of the sedimentary units. Location
312 and stratigraphic position of OSL samples (circled dots) are indicated. OSL data are provided
313 in Table 2. Evidences of individual events (question mark where tenuous, see text for
314 discussion) are labelled with letters. Dashed lines and question marks figure the correlation of
315 events proposed across the five distinctive parts of the trench.
316
317 **Figure 5:** Field photograph showing the upper part of the trench and the east-facing scarp in
318 the background. View to the south with 1.65 m tall geologist for scale. The smooth
319 topography of the scarp contrasts markedly with the rugged set of fissures disrupting a
320 calcrete and filled by recent sediments (aeolian sands and thin slope colluviums of unit 7, see
321 also Figure 4 and Table 1).
322
323 **Figure 6**: Evidence for coseismic deformations. a, 1m-deep fissure disrupting a gypsiferous
324 calcrete developed from colluviums A3. The sandy-silty material of the fissure was emplaced
325 probably during dust winter storms, shortly after the earthquake. The hole, 50 cm below
326 ground surface, locates the OSL sample HI/2006-II. (b), fissure (dark blue flags) filled by
327 sands abutting on f1 fault. (c), Steep faults disrupting coarse alluviums. The middle fault,
328 disrupting an alternation of conglomeratic and sandy-silty layers (D2 unit), is sealed by a
329 colluvium (D3 unit). (d), colluvial wedge (CW, brown horizontal layers, D5 unit)
330 unconformable on 15-20°E dipping alluvial units tilted against a 50°W dipping fault. A
331 fissure filled by gravely material and coarse sands (f, D6 unit) disrupts the colluvial wedge.
332 The fissure and the colluvial wedge have been both indurated by a calcrete pedogenesis and
333 coated by a thin layer of sand and silt.
334
335
336
337
338
339

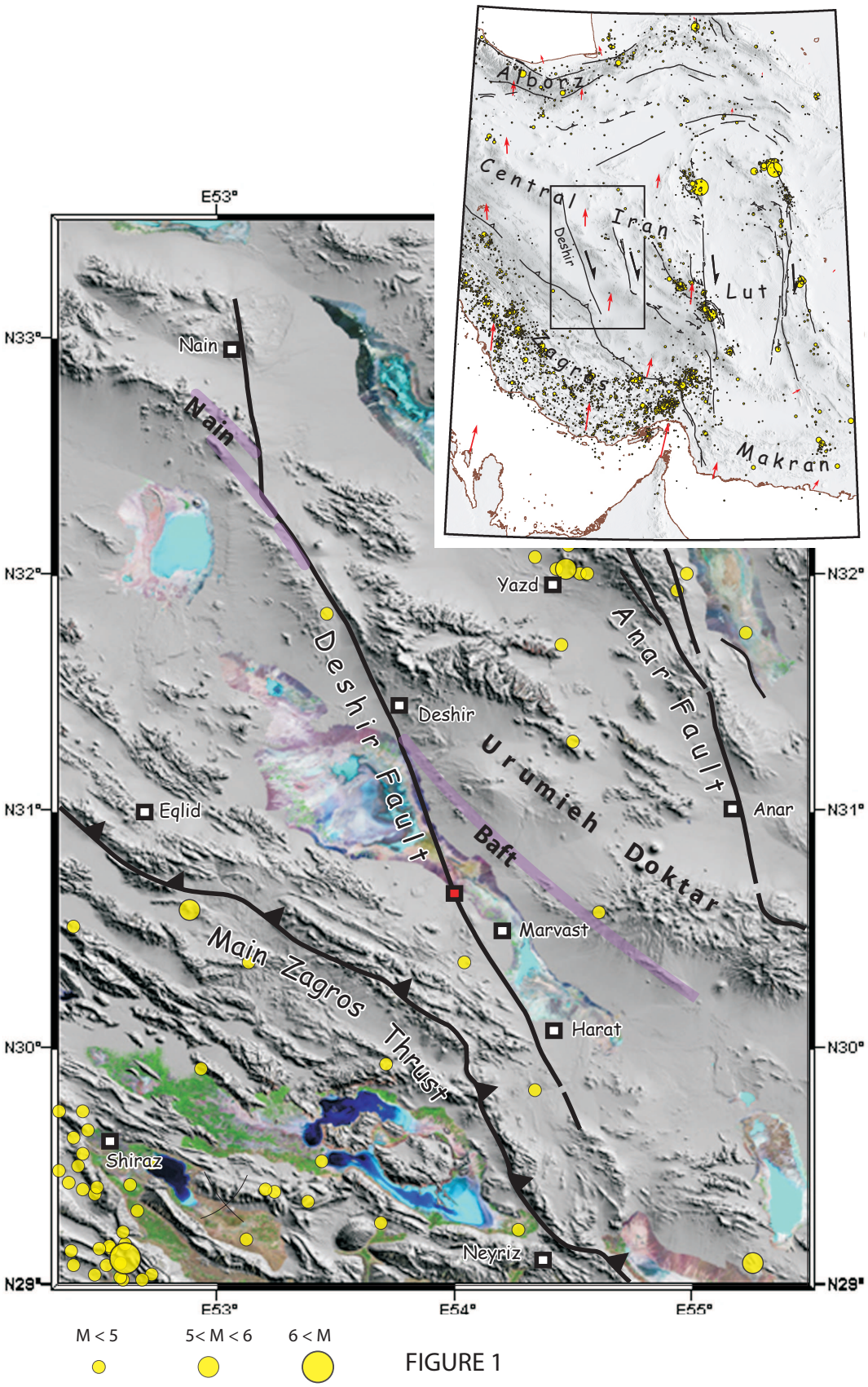
Alborz
Central Iran
Deshir
Lut
Zagros
Makran
E53°
N33°
N32°
N31°
N30°
N29°
Nain
Nain
Deshir Fault
Deshir
Yazd
Anar Fault
Anar
Urumieh Doktar
Baft
Eqlid
Marvast
Main Zagros Thrust
Harat
Shiraz
Neyriz
E54°
E55°
M < 5
5< M < 6
6 < M

FIGURE 1

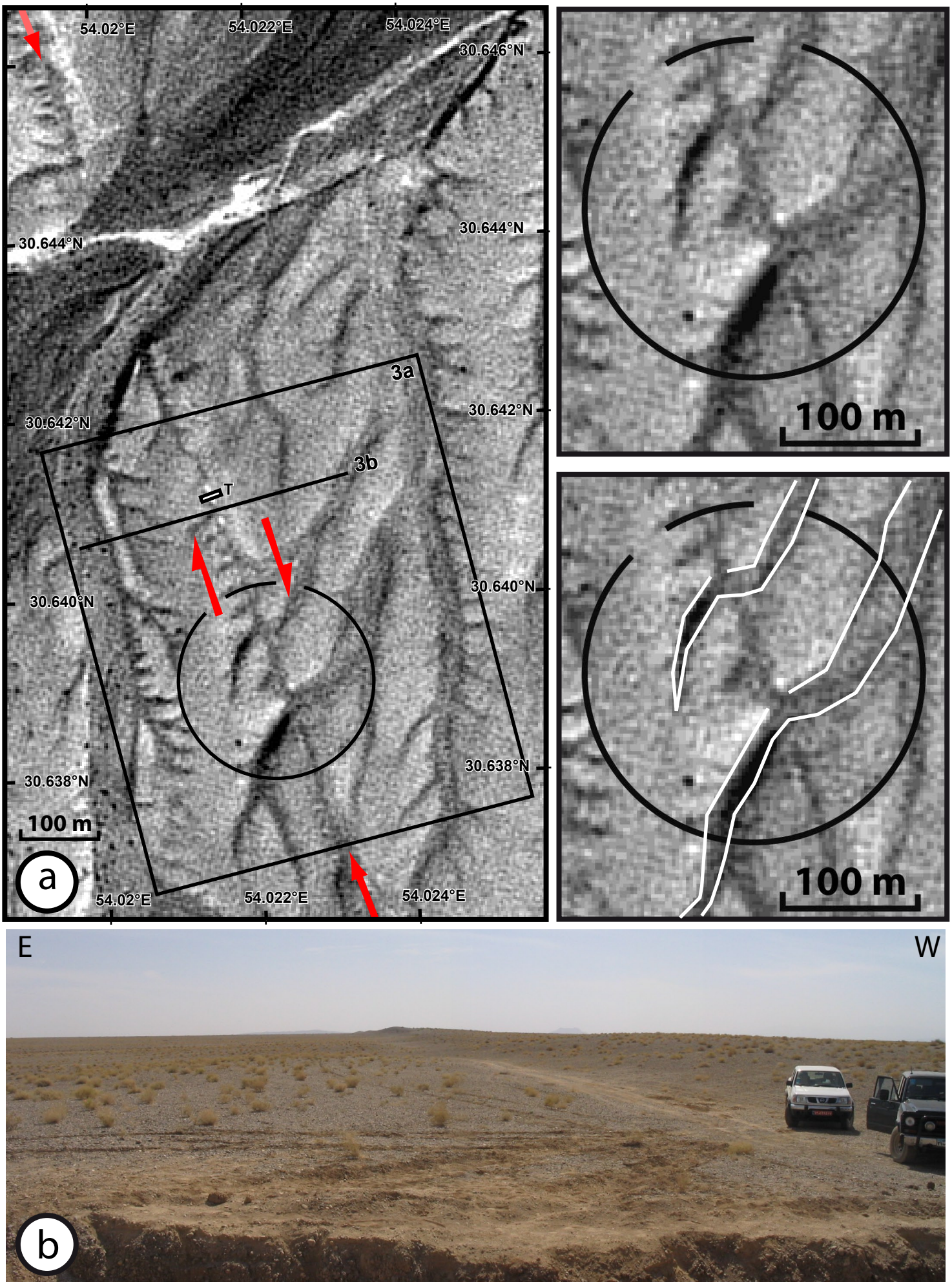
54.02°E
54.022°E
54.024°E
30.646°N
30.644°N
30.644°N
30.642°N
30.642°N
3a
3b
T
30.640°N
30.640°N
30.638°N
30.638°N
100 m
a
54.02°E
54.022°E
54.024°E
100 m
100 m
E
W
b

FIGURE 2

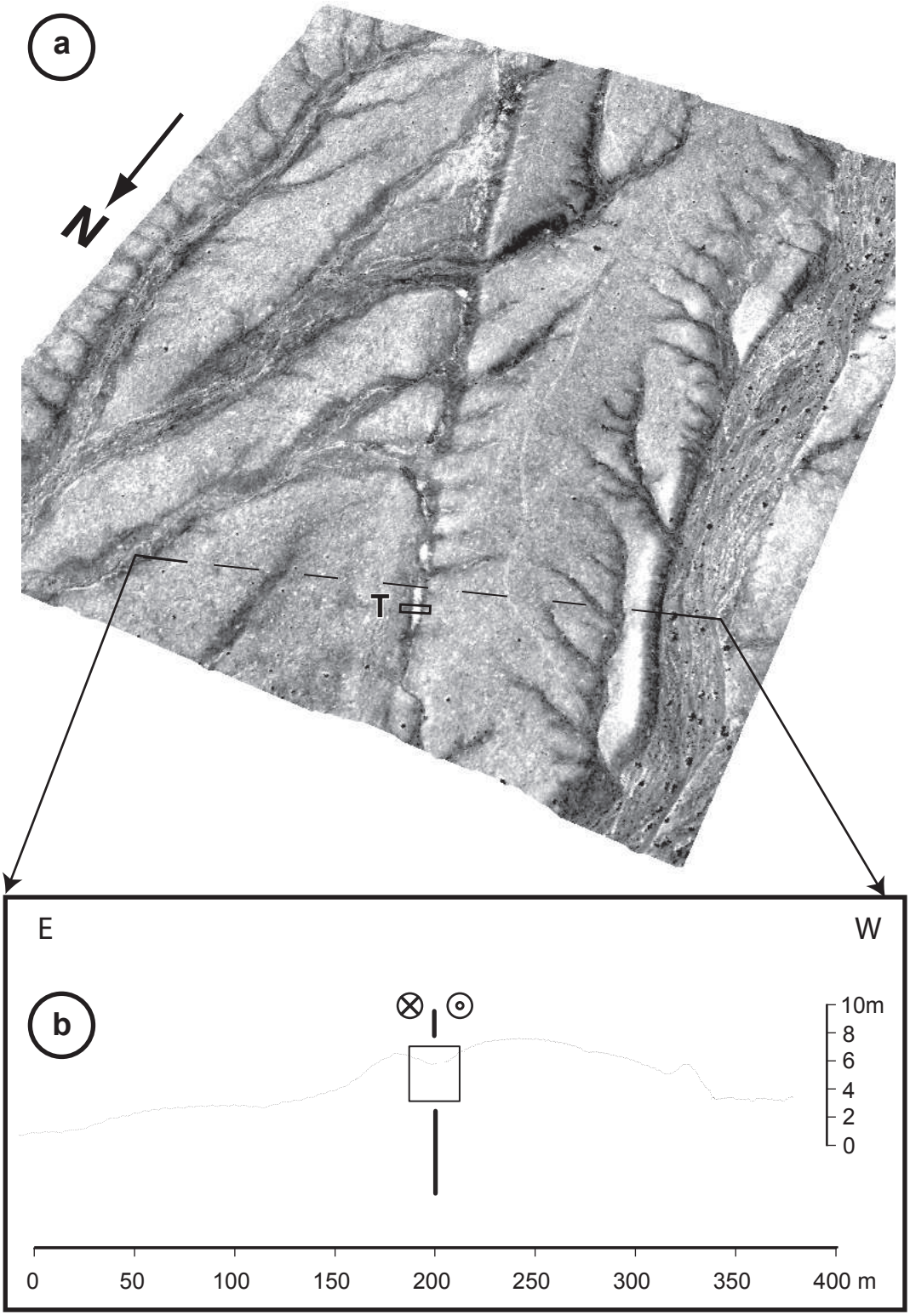

Figure 3

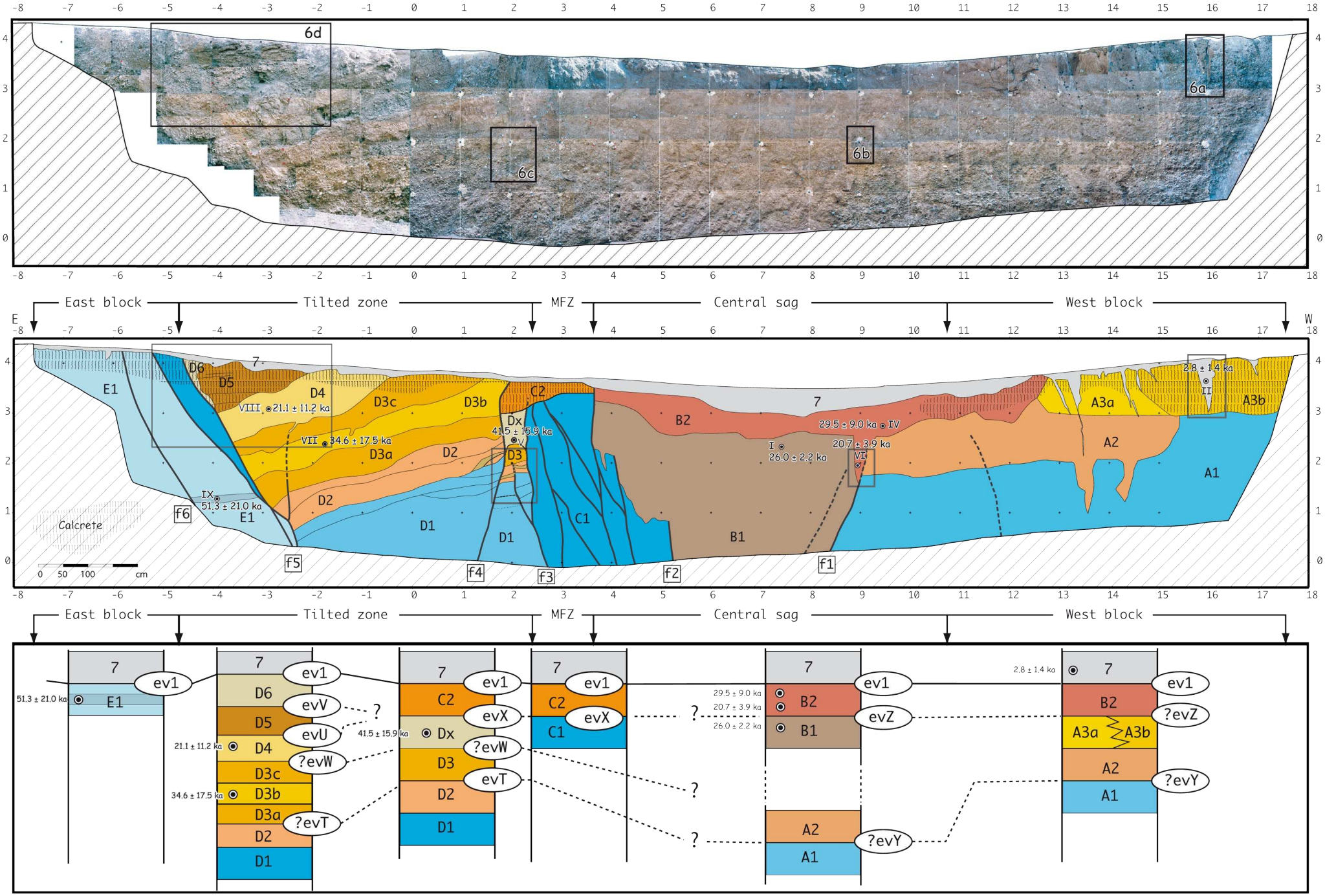
6d
6c
6b
6a
East block
Tilted zone
MFZ
Central sag
West block
E
W
7
D6
D5
D4
D3c
D3b
D3a
D2
D1
E1
C2
C1
Dx
D3
B2
B1
A3a
A3b
A2
A1
VIII 21.1 ± 11.2 ka
VII 34.6 ± 17.5 ka
41.5 ± 15.9 ka
V
29.5 ± 9.0 ka IV
I
26.0 ± 2.2 ka
20.7 ± 3.9 ka
VI
2.8 ± 1.4 ka
II
IX
51.3 ± 21.0 ka
Calcrete
0 50 100 cm
f6
f5
f4
f3
f2
f1
ev1
evV
evU
?evW
?evT
evX
?evW
evT
evZ
?evZ
?evY
?


E
W
Fs

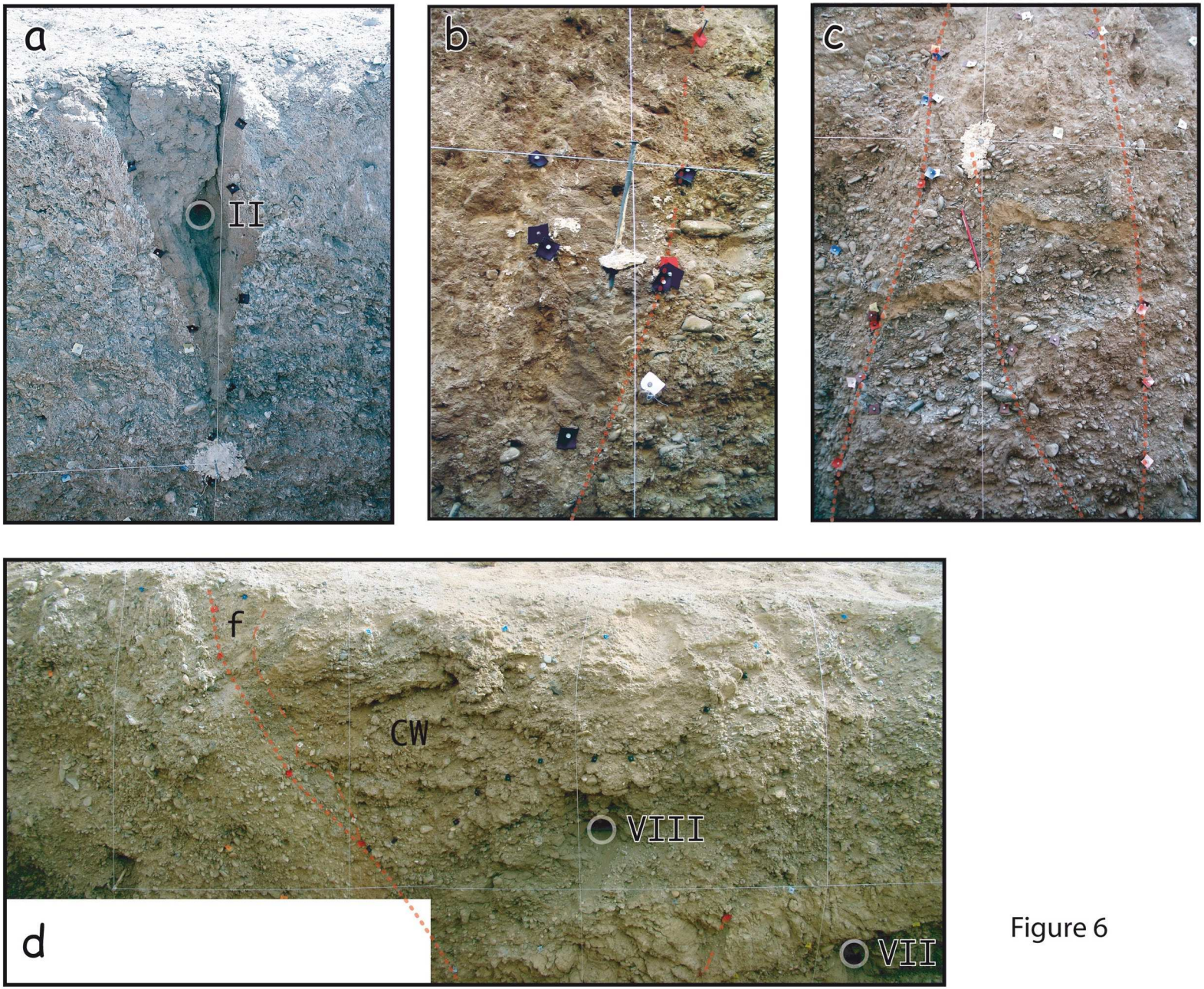

Figure 6

East Block	West Tilted Zone	East Tilted Zone	Main Fault Zone	Central Sag	West Block
7: white-brown colluvial deposit - fair sorting, 2% (Ø 0.2-1cm) clasts, sub-round to round - sandy on trench edges and silty in centre - thin run-off and aeolian deposits filling cracks within calcrete horizon crack infill with **2.8 ± 1.4 OSL ka**					
	D6: coarse fissure fill, non-stratified, 70% (Ø 0.5-2cm) clasts, angular - clay silt and coarse sand matrix - calcrete cementation with gypsum	**C2**: - light grey to beige colluvial deposits - fair sorting, non-stratified - 60% (Ø 0.5-4cm) clasts, sub-round to round - silt and sand matrix - calcrete cementation with gypsum		**B2**: - red to brown alluvial-colluvial deposits - poor sorting, poor stratification, - 20% (Ø 0.5-2cm) clasts - angular to sub-round - silt and sand matrix - **29.5 ± 9 OSL ka** at B2 base - **20.7 ± 3.9 OSL ka** in fissure fill on upper f1 termination	**A3a:** - white to brown colluvium - poor to medium sorting, non-stratified - 20% (Ø 0.5-4cm) clasts, sub-round - silt and sand matrix - calcrete cementation with gypsum.
	D5: brown colluvial wedge deposit - poor sorting, fair stratification - 60% (Ø 0.5-4cm) clasts, angular - strong calcrete cementatation - reworking alluvial material from the East block				**A3b:** - colluvial deposits, sand pebble channel with 80% clasts. - A3a and A3b cut and fill within A2, - belong to the desert colluvial cover of A1 alluvial deposits.
	D4: - grey alluvial material, similar to D3b, - fair sorting, thin stratification - 80% (Ø 0.5-5cm) clasts, sub-round - silt and sand matrix - sand lens with **21.1 ± 11.2 OSL ka**	**Dx:** light grey to beige colluviums - non-stratified fair sorting - 2% (Ø 0.2-1cm) clasts - silt and coarse sand matrix - 41.5 ± 15.9 OSL ka - Dx age bracketed between **25.6 and 57.4 ka**		**B1:** - light red to brown alluvial deposits - poor stratification, poor sorting - 5% (Ø 0.5-4cm) clasts, angular to sub-round - clay silt and sand matrix, gypsum content increases upward - **26 ± 2.2 OSL ka** - B1 top bracketted between **23.8 and 28.2 ka.**	
	D3c: - light brown alluvial deposits - fair sorting, fair stratification - 5% (Ø 0.5-3cm) sub-round clasts in small lenses, clay and silt matrix	D3: - light grey colluvial deposits - poor sorting, non-stratified -30% (Ø 0.2-2cm) angular clasts - clay silt and coarse sand matrix - corresponds to distal runoff material reworking D1 and possibly D2 units close to fault scarp.			**A2:** - light grey to buffish alluvial material - poorly sorting, non-stratified - 25% (Ø 0.5-4cm) clasts, sub-round - silt and clay matrix - channels with higher (35%) clast percentage - cut and fill within highest terrace (A1) - corresponds to mud flow deposits reworking A1
	D3b: grey alluvial material - fair sorting, poor stratification - 85% (Ø 0.5-4cm) clasts, sub-round - silt and sand matrix - sand lens with **34.6 ± 17.5 OSL ka,** indicating D3b age ranging between **17.1 and 52.1 ka.**				
	D3a: - brown alluvial deposits, fair sorting - 5% (Ø 0.5-2cm) clasts, sub-round - clay and silt matrix - similar to D3c.				
E1: - distal alluvial fan deposits corresponding to uppermost terrace level above present-day streams - similar to A1 and D1 - **51.3 ± 21 OSL ka** in a sand lens between f5 and f6 indicating age ranging between 30.3 and 72.3 ka	**D2**: grey to light brown alluvial material, dark level for red-brown sands - fair sorting, fair stratification - 80% (Ø 0.2-7cm) clasts, sub-round to round - clay silt and sand matrix, less cemented and more layered than D1 - overlying D1 without noticeable unconformity - corresponds to remnants of intermediate alluvial terrace younger than A1 D1 and E1 and emplaced approximately parallel to Deshir fault		**C1:** - alluvial material similar to A1, D1, and E1 - (50%) clasts - unit highly sheared and disrupted showing broken clasts oriented parallel to f2-f3 zone		**A1:** - grey to brown alluvial material - poor-medium sorting, poor stratification - 80% (Ø 0.5-10cm) clasts, sub-round to round - clay silt and sand matrix - carbonate cementation and gypsum - correspond to distal alluvial fan deposits of the uppermost terrace level observed above present-day streams.
	D1: alluvial deposit similar to A1 and E1				

Table 1: Description of the sedimentary units observed within the Deshir trench (see Figure 4). Block names are in column headers and unit names are indicated in bold. Thin black lines are either block limits (vertical) or boundary between units (horizontal). Thick continuous black lines figure confidently determined event horizons of earthquake while thick dotted-dashed lines represent questionable event horizon.

Table 2: Optically Stimulated Luminescence ages for the Deshir samples. Age determination requires knowledge of the equivalent (D_e) and annual (D_a) doses for each sample. Ages have been calculated for Quartz grains with size ranging between 90 and 250 microns.

Sample [a]	Unit	Equivalent Dose De (Grays) [b]	depth (m)	Water (%)	K [c] (%)	U [c] (ppm)	Th [c] (ppm)	Annual Dose rate Da (Grays/ka)[d]	Age (ka) [e]
HI/2006-I	B1	60.16 ± 4.60	1.2	0.9	1.22 ± 0.01	1.79 ± 0.05	6 ± 0.1	2.31 ± 0.06	26.0 ± 2.2
HI/2006-II	7	5.00 ± 2.37	4	1.1	0.73 ± 0.01	1.67 ± 0.05	5.5 ± 0.1	1.76 ± 0.04	2.8 ± 1.4
HI/2006-IV	B2	70.21 ± 21.24	0.8	1.2	1.2 ± 0.01	2.09 ± 0.05	6 ± 0.1	2.38 ± 0.06	29.5 ± 9.0
HI/2006-V	Dx	81.97 ± 31.23	1.3	1.0	0.98 ± 0.01	1.47 ± 0.05	5.9 ± 0.1	1.98 ± 0.05	41.5 ± 15.9
HI/2006-VI	B2	50.14 ± 9.26	1.5	1.3	1.27 ± 0.01	2.04 ± 0.05	6 ± 0.1	2.42± 0.06	20.7 ± 3.9
HI/2008-VII	D3b	47.00 ± 23.79	1.6	1.1	0.61 ± 0.01	1.1 ± 0.05	4.3 ± 0.1	1.36 ± 0.03	34.6 ± 17.5
HI/2008-VIII	D4	30.64 ± 23.77	0.95	0.9	0.66 ± 0.01	1.13 ± 0.05	4.6 ± 0.1	1.45 ± 0.03	21.1 ± 11.2
HI/2008-IX	E1	71.63 ± 29.22	2.8	1.2	0.66 ± 0.01	1.12 ± 0.05	4.5 ± 0.1	1.40 ± 0.03	51.3 ± 21.0

[a] The samples were collected using stainless steel tubes (5 cm by 25 cm) and both ends were sealed and covered using both aluminium foil and black tape. Quartz was extracted from all samples using standard methods in the Sheffield Centre for International Drylands Research Centre Luminescence Laboratory (see Bateman and Catt (1996) for details)

[b] Luminescence measured through 7 mm Hoya U-340 filters in a Risø (Model TL/OSL-DA-15) automated TL/OSL system. The equivalent dose (D_e) was obtained using the conventional quartz single aliquot regeneration method (Murray and Wintle, 2000)

[c] Uranium, thorium and potassium concentrations were measured using inductively coupled plasma mass spectrometer (ICP-MS) at SGS laboratories Ontario, Canada.

[d] The annual dose (D_a) was estimated from these data and the cosmic ray contributions as described in Fattahi et al. (2006 and 2007).

[e] errors are 1 sigma